Electrochimica Acta 246 (2017) 870–878

Contents lists available at ScienceDirect

Electrochimica Acta

journal homepage: www.elsevier.com/locate/electacta

The Pseudocapacitive Nature of $CoFe_2O_4$ Thin Films

Jagdeep S. Sagu[a], K.G.U. Wijayantha[a,*], Asif A. Tahir[b]

[a] Energy Research Laboratory (ERL), Department of Chemistry, Loughborough University, Loughborough, LE11 3TU, UK
[b] Environment and Sustainability Institute (ESI), University of Exeter Penryn, Cornwall TR10 9FE, UK

ARTICLE INFO

Article history:
Received 19 April 2017
Received in revised form 19 June 2017
Accepted 19 June 2017
Available online 20 June 2017

Keywords:
Supercapacitor
Pseudocapacitance
Thin film
Metal oxide

ABSTRACT

Nanostructured Cobalt ferrite ($CoFe_2O_4$) thin films are fabricated by aerosol-assisted chemical vapour deposition (AACVD) and studied for application in supercapacitors. XRD and Raman spectroscopic analysis confirms the formation of single phase $CoFe_2O_4$. SEM analysis shows that the thin film morphology consists of nanoparticles less than 100 nm in size that are sintered together to form larger dendrites raised from the substrate. The larger dendrites range from 0.5–1 μm in diameter and are uniformly distributed over the FTO substrate, providing a highly porous structure which is desired for supercapacitor electrodes. Three-electrode electrochemical measurements reveal that $CoFe_2O_4$ is pseudocapacitive and is highly conducting. Studies of $CoFe_2O_4$ thin films in two-electrode symmetric supercapacitor configuration show a capacitance of 540 $\mu F\,cm^{-2}$ and a relaxation time constant of 174 ms. Around 80% of the capacitance is retained after 7000 charge-discharge cycles when a maximum charging voltage of 1 V was used, indicating that the pseudocapacitive processes in $CoFe_2O_4$ are highly reversible and that it exhibits excellent chemical stability in 1 M NaOH alkaline electrolyte solution. The results show that $CoFe_2O_4$ is a cheap and promising alternative pseudocapacitive material to replace the expensive pseudocapacitive materials.

1. Introduction

Supercapacitors are energy storage devices which offer high power densities, excellent cycling stabilities (>10000 cycles) and fast charging rates. In certain applications in which the energy demand is sufficiently low and power demand is high, supercapacitors have already started to replace batteries, for example, they have been used in electric power tools, phone chargers and portable vacuum cleaners. Their main advantages are that they can be fully charged in minutes rather than hours, as with batteries, and they have high power density. Unfortunately, the major limiting factor for the application of supercapacitors in place of batteries is their lower energy densities by comparison. As the energy stored in a supercapacitor is proportional to the square of the operating voltage, a significant effort has gone into designing new electrolytes with large electrochemical stability windows, e.g. ionic liquids. Another strategy has been to try and increase the overall capacitance of the electrode material.

Generally, there are two mechanisms of energy storage in a supercapacitor: through the electrochemical double-layer or by faradaic charge transfer across the electrode-electrolyte interface, termed pseudocapacitance. The majority of commercially available supercapacitors use carbon-based high surface area electrodes, where 95-99% of the overall charge storage stems from the double layer. By contrast, pseudocapacitors can store up to hundred times more charge per unit surface area than that of double layer capacitance, due to the nature of charge storage mechanism [1]. However, generally, pseudocapacitor materials tend to have shorter cycling lifetimes due to the redox reactions not being completely reversible or disintegration of the crystal structure due to repeated ingression/egression of counter ions, causing loss of electrical contact and therefore reduced charge storage; although this can be reduced by combining the pseudoactive material with a conductive support [2]. Thus, pseudocapacitive electrode materials that also possess good chemical stability have currently received significant attention. Metal oxides, such as MnO_2 [3], IrO_2 [4], V_2O_5 [5] and RuO_2 [6] have previously been studied for use in pseudocapacitors as they all have multiple oxidation states to facilitate faradaic charge transfer. Among them, only oxides of precious metals such as IrO_2 and RuO_2 have shown good chemical stability, but they are

* Corresponding author.
E-mail address: u.wijayantha@lboro.ac.uk (K.G.U. Wijayantha).

http://dx.doi.org/10.1016/j.electacta.2017.06.110

very expensive. MnO_2 is an alternative to IrO_2 and RuO_2 because it is much lower in cost, less toxic and has high theoretical capacitances ranging from 1100 to 1300 F/g [7–11]. The main limiting factor for the use of MnO_2 as a pseudocapacitor material is its poor cycling stability [8]. Other materials have not yet shown the potential to withstand the sufficient stability challenge in order to use them in commercially viable devices. Hence, the search for alternative low-cost materials with promising pseudocapacitive properties is a hot topic in the area of supercapacitor development today.

Spinel ferrites can be potential candidate materials as they are stable, abundant, inexpensive and are environmentally friendly. Spinel ferrite thin films, with the general structure MFe_2O_4 (where M = Ni^{2+}, Co^{2+}, Zn^{+} and Cu^{2+} etc.) have been attracting great interest for wide range of electronic applications such as magnetic tunnel junctions (MTJs), magnetic random access memories (MRAMs), spin valves, resistive random access memories (RRAMs), microwave devices and sensors [12–18], as well as catalysts [19]. This is due to their unique properties such as high coercivity, moderate saturation magnetization, high magnetocrystalline anisotropy, mechanical and excellent chemical stability [20]. For these reasons, there have been more studies on the use of spinel ferrite materials for application in supercapacitors recently. $MnFe_2O_4$ [21–23], $NiFe_2O_4$ [24], $ZnFe_2O_4$ [25,26], $CuFe_2O_4$ [27] and $CoFe_2O_4$ [28–31] are amongst the materials already investigated. $CoFe_2O_4$ has demonstrated gravimetric capacitances ranging from 142 Fg^{-1} to 768 Fg^{-1} and has shown capacitance retention of 79.2% after 5000 charge-discharge cycles [28,29,31]. Also, cobalt ferrite ($CoFe_2O_4$) has been recently studied as an oxygen evolution reaction (OER) catalyst and it was found to be very stable in alkaline solutions [32]. Due to the excellent electrochemical stability demonstrated by $CoFe_2O_4$, it warrants further research to determine its potential as a supercapacitor electrode material if highly porous electrodes can be prepared by a suitable low-cost route (to increase the double layer capacitance) and stable surface redox groups are present (to incorporate pseudocapacitance properties).

New materials which possess true pseudocapacitance (i.e. exhibit pseudo-rectangular cyclic voltammograms) are rare. There has been some controversy in the literature regarding the use of the term 'pseudocapacitance' for many transition metal oxides and hydroxides such as NiO or $Ni(OH)_2$ and Co_3O_4 or $Co(OH)_2$, as well as the calculations used to determine their capacitance. Nickel and cobalt oxides/hydroxides have been reported to have very high specific capacitances of over 1000 Fg^{-1}, however, these materials exhibit peak shaped cyclic voltammograms, which have led to over estimations of their capacitances as well as confusion between capacitive and non-capacitive processes [33]. Herein, we report the pseudocapacitive nature of $CoFe_2O_4$ thin films and present an in-depth study of the electrochemical characteristics of the thin film electrodes in order to demonstrate the suitability of $CoFe_2O_4$ as an active electrode material in supercapacitors. Three-electrode electrochemical measurements revealed that $CoFe_2O_4$ is truly pseudocapacitive, exhibiting pseudo-rectangular cyclic voltammograms. $CoFe_2O_4$ tested in a two-electrode symmetric supercapacitor configuration showed a capacitance of 540 $\mu F\,cm^{-2}$ and a relaxation time constant of 174 ms. The supercapacitor showed remarkable stability with only 20% loss in capacitance after 7000 cycles indicating that the pseudocapacitive processes in $CoFe_2O_4$ are highly reversible and exhibit excellent electrochemical stability in alkaline electrolyte (1 M NaOH). We attribute the origin of pseudocapacitance to both FeOOH and CoOOH surface groups which are known to be redox active.

2. Experimental

2.1. Preparation of AACVD precursor solution and deposition of $CoFe_2O_4$ thin film electrodes by AACVD

A precursor solution containing iron (III) acetylacetonate (0.1 M) and cobalt (II) acetate (0.05 M) was made up in methanol and stirred for 30 min. Thin film electrodes of $CoFe_2O_4$ were deposited by AACVD onto fluorine-doped SnO_2 (FTO) conducting glass substrates (TEC 8 NSG, 8 $\Omega/\square$). Prior to the deposition, the FTO glass substrates were cut to a 1 cm x 2 cm size and were ultrasonically cleaned with distilled water, acetone, isopropanol and then were stored in ethanol. The substrates were dried in air prior to the deposition and placed on a hot plate. The glass substrates were heated for at least 10 min to allow the substrate temperature to be equilibrated with that of the surface of the hotplate. A flask containing the precursor solution was placed above the piezoelectric modulator of an ultrasonic humidifier to generate aerosol droplets of precursor. Air at the rate of 175 ml min^{-1} was used as the carrier gas to transfer the aerosol to the deposition chamber through a second flask, where the large droplets were filtered from the aerosol stream at a flow rate of 2340 ml min^{-1}, allowing only the fine aerosol droplets to be transferred to the deposition chamber. In order to study the effect of deposition temperature on electrode performance, the depositions were carried out at temperatures of 450, 500 and 550 °C for 20 mins and prepared series of electrodes. After each deposition was completed, the coated FTO substrates were removed from the deposition chamber and allowed to cool to room temperature. The background theory, deposition mechanism and extensive experimental details of the AACVD process for the fabrication of thin films are described in more detail elsewhere [34,35].

2.2. Material Characterization

The phase and crystallinity of the films were characterized using a Bruker AXS Advance X-ray diffractometer with primary monochromatic high intensity Cu Kα (λ = 1.541 Å) radiation. Raman spectra were recorded using a HORIBA Jobin Yvon LabRAMHR Raman spectrophotometer (with 632.8 nm He–Ne laser). The surface morphology of the thin films were investigated using a field emission gun scanning electron microscopy (FEG-SEM, Leo 1530 VP) at aen accelerating voltage of 5 kV and working distance of 5 cm. XPS measurements were conducted using a Thermo Scientific (model K-Alpha) spectrometer.

2.3. Electrochemical Characterization

All electrochemical measurements were carried out using an Autolab PGSTAT12 potentiostat. Three-electrode measurements were conducted in 1 M NaOH using a Pt gauze counter electrode and Ag|AgCl reference electrode in a sealed vessel after purging the electrolyte solution with argon for 20 min prior to any electrochemical measurement. The reference potential of the Ag|AgCl electrode was checked before and after electrochemical measurements to ensure a stable reference potential. The potential of the Ag|AgCl reference electrode was indeed stable over the course of the measurements. Prior to construction of two-electrode supercapacitors, two $CoFe_2O_4$ electrodes and a filter paper (which was used as the separator) were soaked in 1 M aqueous NaOH electrolyte in order to wet them completely. The separator was sandwiched between the two $CoFe_2O_4$ electrodes and was clamped together with clips. For all cyclic voltammetry experiments, three scans were obtained, only the third scan is presented in the data. For stability measurements, the cell was sealed using PTFE tape to prevent evaporation of the solvent. Cyclic voltammetry

measurements were carried out at various scan rates between the voltage window of 0 and 1 V. Scan rates were maintained between 0.1 and 15 V/s. Galvanostatic charge-discharge measurements were carried out at various charging currents (40–120 μA) between 0 and 1 V. The capacitance was determined from the slope of the discharge curve, after the initial potential drop due to internal resistance [36]. The maximum energy stored, E, and power delivered, P, was determined from Eqs. (1) and (2):

$$E = \frac{1}{2}CV^2 \quad (1)$$

$$P = \frac{V^2}{4R_s} \quad (2)$$

where V is the maximum cell voltage (taken to be 1 V), C is the capacitance and R_s is the equivalent series resistance (ESR). Stability – lifetime measurements were carried out for 7000 charge-discharge at a maximum charging voltage of 0.8 V and 1 V. Electrochemical impedance spectroscopy (EIS) of the supercapacitor was carried out at 0 V in the frequency range 0.01 Hz to 10 kHz with 10 mV amplitude. Three-electrode mode EIS measurements were conducted at open-circuit potential.

3. Results and Discussion

AACVD of a methanolic precursor solution containing iron (III) acetylacetonate and cobalt (II) acetate resulted in brown/black colored films when depositions were conducted at 450, 500 and 550 °C (see the inset of Fig. 3a to c). The phase and crystallinity of the deposited films were characterized by XRD, as shown in Fig. 1a. The color of all three $CoFe_2O_4$ films were visually similar, and the film prepared at 450 °C only showed reflections which corresponded to the F:SnO_2 substrate. The peaks at 26.8°, 34.0°, 38.0°, 51.7°, 54.7°, 61.7° and 65.7° correspond to the (110), (101), (111), (211), (220), (310) and (301) reflections of SnO_2, respectively (ICDD 00-041-1445). This indicates that the film prepared at 450 °C was amorphous. When AACVD was carried out at higher temperatures (500 and 550 °C), the film XRD patterns showed the presence of a $CoFe_2O_4$ phase with a cubic crystal structure (ICDD 00-022-1086). The peaks at 18.3°, 30.2°, 35.5°, 43.2°, 57.1°, and 62.7° correspond to the (111), (220), (311), (400), (511), and (440) reflections of $CoFe_2O_4$. The films generally showed a preferred orientation in the (311) direction, as is the case for many other reports of thin film $CoFe_2O_4$ [37–39]. The XRD reflections match very well with literature reported values for $CoFe_2O_4$ [40,41]. The Raman spectra of all three films are shown in Fig. 1b. Raman peaks are seen at 296, 465, 600 and 660 cm^{-1}, which are all characteristic of $CoFe_2O_4$ [42]. No XRD or Raman evidence was observed for common impurity phases such as Co_3O_4 and α-Fe_2O_3, which indicated that a phase pure material had been fabricated in the bulk.

In order to gain an insight of the surface composition of $CoFe_2O_4$ thin films, they were subjected to EDX analysis; the EDX spectra are shown in Fig. S1 of the supporting information. The expected stoichiometric ratio of Co:Fe on the surface of $CoFe_2O_4$ is 0.5, however the observed Co:Fe ratio on the film surface varied with the deposition temperature. The observed ratio for the 450 °C deposited film was 0.46 which was closest to the expected stoichiometric ratio of 0.5. This increased to 0.62 and then to 0.85 at 500 and 550 °C, respectively, indicating that higher deposition temperatures resulted in a Co rich surface. An XPS spectrum (Fig. 1c) of the $CoFe_2O_4$ thin film prepared at 550 °C was measured to determine the oxidation state of the Co species on the Co rich surface. The Co2p spectrum showed two peaks at 780.08 and 795.88 eV, with two satellite peaks at 786.38 and 802.78 eV. Pure

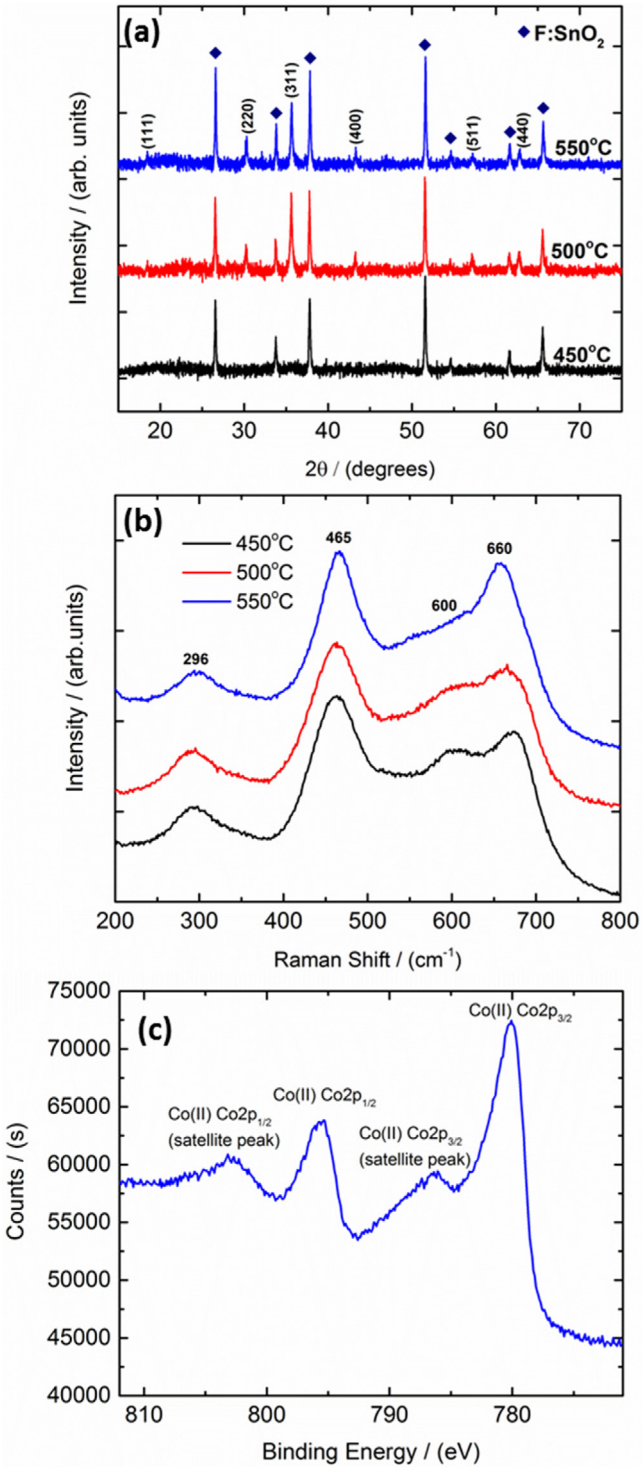

Fig. 1. XRD patterns (a) and Raman spectra (b) of $CoFe_2O_4$ thin films deposited on FTO glass substrates at 450, 500 and 550 °C by AACVD. (c) XPS spectrum of a $CoFe_2O_4$ prepared at 550 °C (Co rich surface).

Co^{2+} can be distinguished from a mixed Co^{2+}/Co^{3+} or pure Co^{3+} oxidation state by the binding energy and intensity of the satellite peaks. The binding energy and intensity of the satellite peaks in this sample are characteristic of pure Co^{2+}, which has distinct satellite peaks at 786.38 and 802.78 eV [43,44]. Pure Co^{3+} usually only shows a weak satellite peak at around 791 eV, whereas a plateau is observed in the region between 791 and 785 eV if both oxidation states are present [43,44]. Therefore, the XPS spectrum

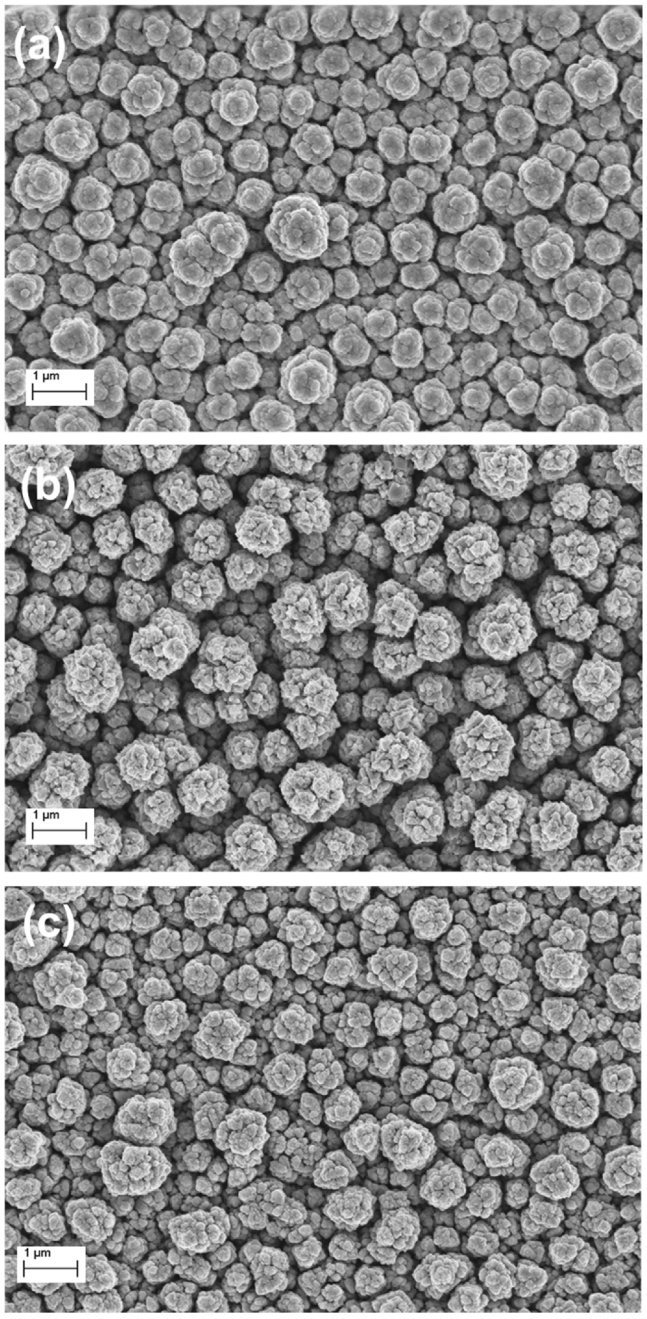

Fig. 2. Surface topographical SEM images of $CoFe_2O_4$ thin films deposited on FTO glass substrates for 20 min using AACVD at (a) 450 °C, (b) 500 °C and (c) 550 °C.

confirms the presence of Co^{2+} on the surface which suggests that the excess Co on the surface could be in the form of $Co^{(II)}Fe^{(III)}O_4$ (as expected) or CoO.

The surface topographical SEM images for the $CoFe_2O_4$ thin films fabricated at 450, 500 and 550 °C are shown in Fig. 2 for a deposition time of 20 min. Generally, the thin film morphology consisted of nanoparticles less than 100 nm in size that are sintered together to form larger dendrites raised from the FTO substrate. The larger dendrites ranged from 0.5–1 μm in diameter and are uniformly distributed over the substrate, providing a highly porous structure which is desirable for supercapacitor electrodes. Electrodes with such a highly porous dendrite structure have been already reported for other materials such as α-Fe_2O_3 and $ZnFe_2O_4$ by the AACVD technique [45,46]. Cross-sectional SEM images can be seen in Fig. S3 in the supporting information.

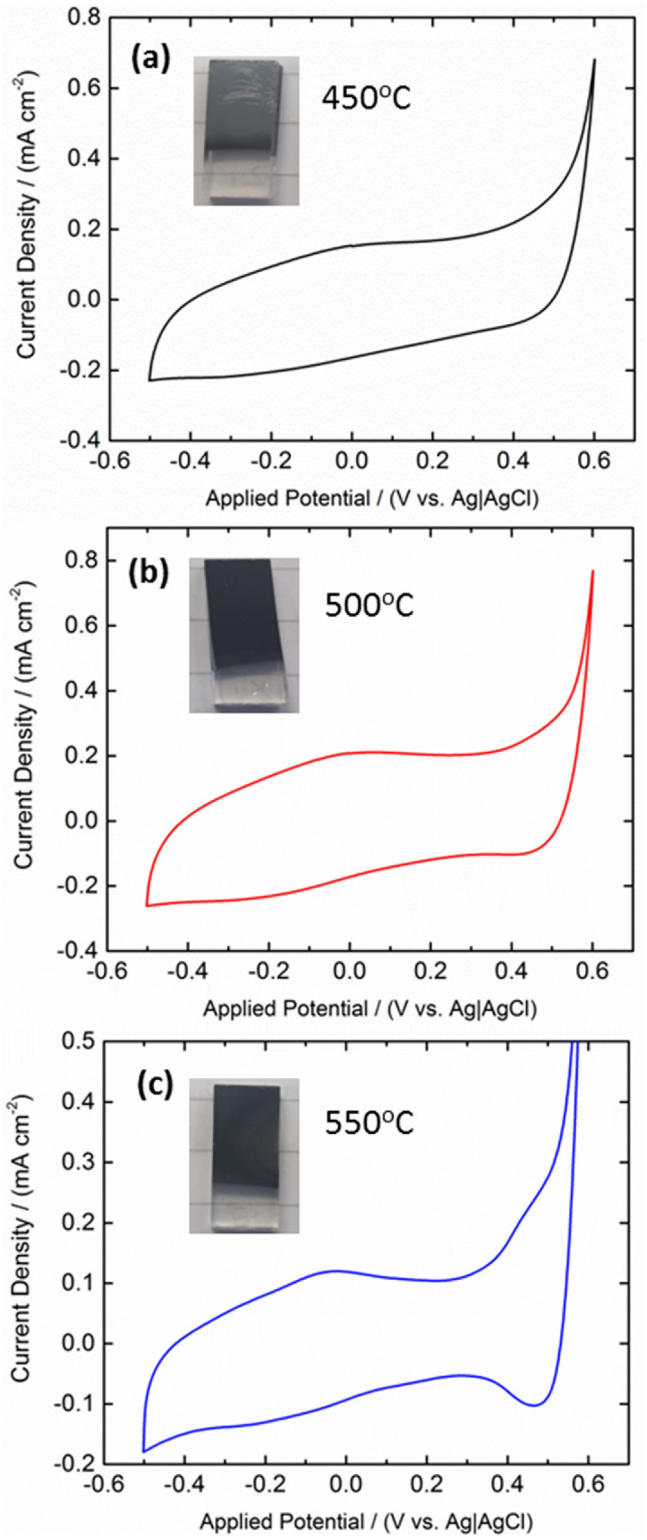

Fig. 3. Cyclic voltammograms of $CoFe_2O_4$ thin films prepared at 450, 500 and 550 °C. Measurements were conducted in 3-electrode mode in 1 M NaOH using a Pt gauze counter electrode and Ag|AgCl reference electrode at a scan rate of 100 mV s^{-1}. The insets show the appearance of the $CoFe_2O_4$ thin films deposited at the respective temperatures.

The electrochemical response of the $CoFe_2O_4$ electrodes prepared at all three different temperatures (450, 500 and 550 °C) are shown in Fig. 3a, b and c, respectively. A photograph of the corresponding film is included in the inset of each figure

showing the color appearance of each film. The $CoFe_2O_4$ thin films prepared at 450 °C contained cracks, as shown in the inset of Fig. 3a, indicating weak adherence of the $CoFe_2O_4$ layer onto the FTO substrate. This film was not only loosely adhered to the substrate but was also mechanically very weak. This could be due to the differences in the AACVD growth mechanism at lower temperatures i.e. the homogeneous or heterogeneous reaction pathway [47,48]. The films deposited at temperatures of 500 and 550 °C have shown excellent adherence by withstanding the 'scotch tape test' indicating a very strong bond between the $CoFe_2O_4$ layer and the substrate. The anodic tail seen at the highest positive potential for each CV (at 0.6 V vs Ag/AgCl) is due to the oxygen evolution reaction [32]. The CVs of all three electrodes contain redox features demonstrating the pseudocapacitive nature of the $CoFe_2O_4$. The EDX spectra of the $CoFe_2O_4$ thin films confirmed the presence of Fe and Co on the surface for films prepared at all three temperatures (450, 500 and 550 °C). The anodic peak observed at −0.02 V for all three $CoFe_2O_4$ electrodes could be due to the oxidation of Fe(II) in the spinel structure to Fe (III), most likely in the form of FeOOH surface species as described by others [31,49,50]. The corresponding cathodic peak for this process is not clearly distinguishable, but appears to exist around −0.3 V (this cathodic peak can be easily identifiable by plotting the first derivative of current versus voltage, which was not shown). The electrodes deposited at 450 °C and 500 °C do not show any other redox features. However, the CV of the $CoFe_2O_4$ thin film prepared at 550 °C shows another clear anodic peak at 0.5 V (Fig. 3c), with a corresponding reduction peak distinguishable at 0.45 V on the reverse scan. From the EDX data (Fig. S1), it was observed that the films prepared at 550 °C had an excess of Co on the surface (~Co:Fe ratio of 0.85), which is most likely due to the presence of CoO_x species on the surface. Therefore, the anodic peak at 0.5 V could be attributed to the oxidation of CoO_x to CoOOH with the corresponding cathodic peak at 0.45 V presumably due to the reduction of CoOOH back to CoO_x [31,51]. The observed Co (II)/(III) redox peaks occur at more positive potentials to those reported in the literature for Co_3O_4–this positive shift can be caused by the influence of Fe in the structure [52]. The redox peaks for the CoO_x surface species were only observed for the film prepared at 550 °C. As discussed earlier, the $CoFe_2O_4$ film prepared at 450 °C showed a Co:Fe ratio of 0.46, which was the closest to the ideal Co:Fe ratio of 0.5 on the surface in our study. Unfortunately, due to poor film adherence and cracks, this electrode could not be used for further electrochemical analysis. The electrochemical response of the film prepared at 500 °C was similar to that of the film prepared at 450 °C. It did not show any electrochemical evidence for the presence of surface CoO_x species although excessive Co was determined on the surface from the EDX measurements (Co:Fe ratio was estimated to be 0.62). For this reason, the $CoFe_2O_4$ thin films prepared at 500 °C were used for further electrochemical analysis in a two-electrode configuration. The CVs of the $CoFe_2O_4$ thin films prepared at 450 °C and 500 °C were pseudo-rectangular within a potential window of 1 V (-0.5 V to +0.5 V vs. Ag|AgCl), therefore, the $CoFe_2O_4$ thin films can be considered pseudocapacitive.

As the XRD patterns of $CoFe_2O_4$ thin films prepared at all three temperatures showed reflections from the substrate (FTO), the electrochemical response of the bare substrate was compared with a typical $CoFe_2O_4$ thin film to ensure the electrochemical responses observed in Fig. 3 were purely from the $CoFe_2O_4$ thin film and not from the substrate. Fig. S6 shows that the electrochemical response of the FTO substrate is negligible compared to a typical $CoFe_2O_4$ film, therefore, it can be assumed that the electrochemical responses of electrodes in Fig. 3 are purely from $CoFe_2O_4$.

In order to gain further insight in to the $CoFe_2O_4$ film porosity and conductivity, Nyquist plots were recorded in 3-electrode mode

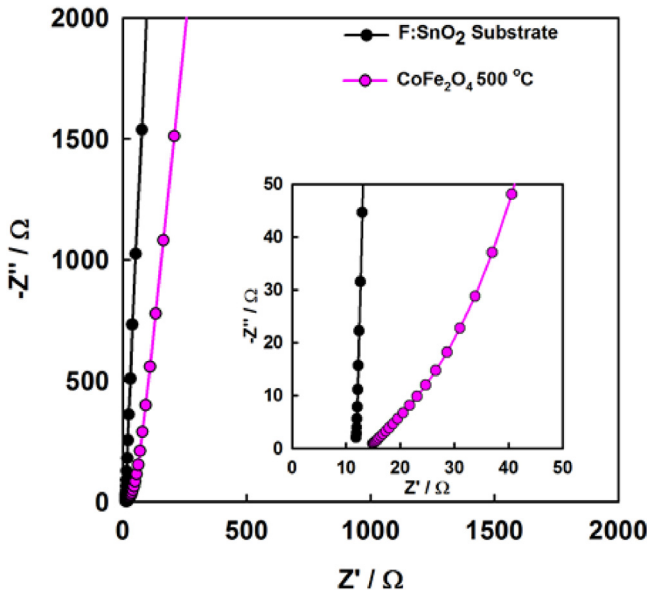

Fig. 4. Nyquist plots recorded for a bare FTO substrate (black) and a $CoFe_2O_4$ film prepared at 500 °C on an identical FTO substrate (purple). Measurements were conducted in 3-electrode mode in 1 M NaOH using a Pt gauze counter electrode and Ag|AgCl reference electrode at open circuit potential in the frequency range of 0.01 Hz to 10 kHz.

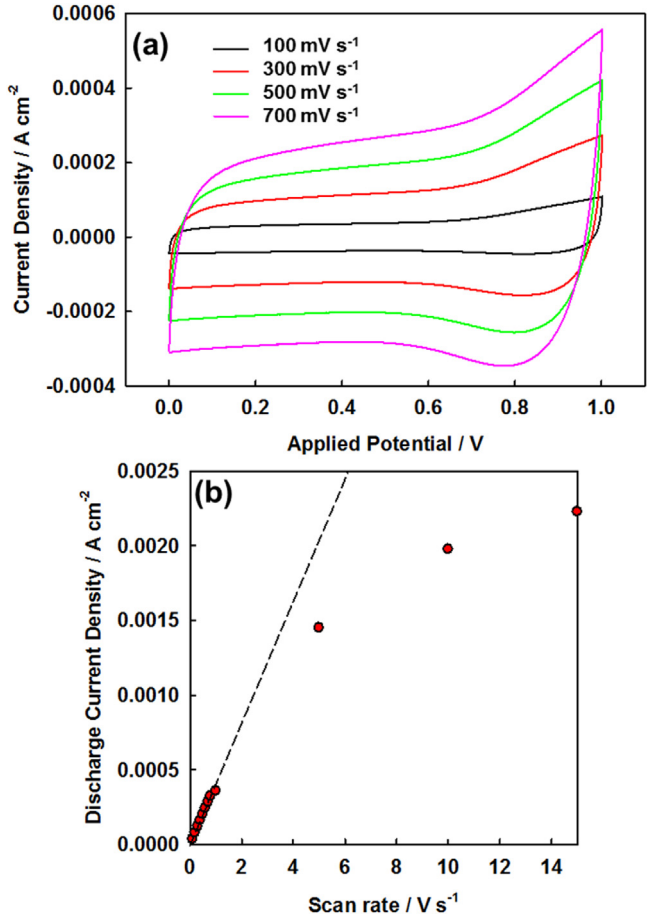

Fig. 5. (a) Cyclic voltammograms of a $CoFe_2O_4$ symmetric supercapacitor in 1 M NaOH at various scan rates. (b) Plot of discharge current density (determined from the reverse scan of CV at 0.5 V) vs. scan rate.

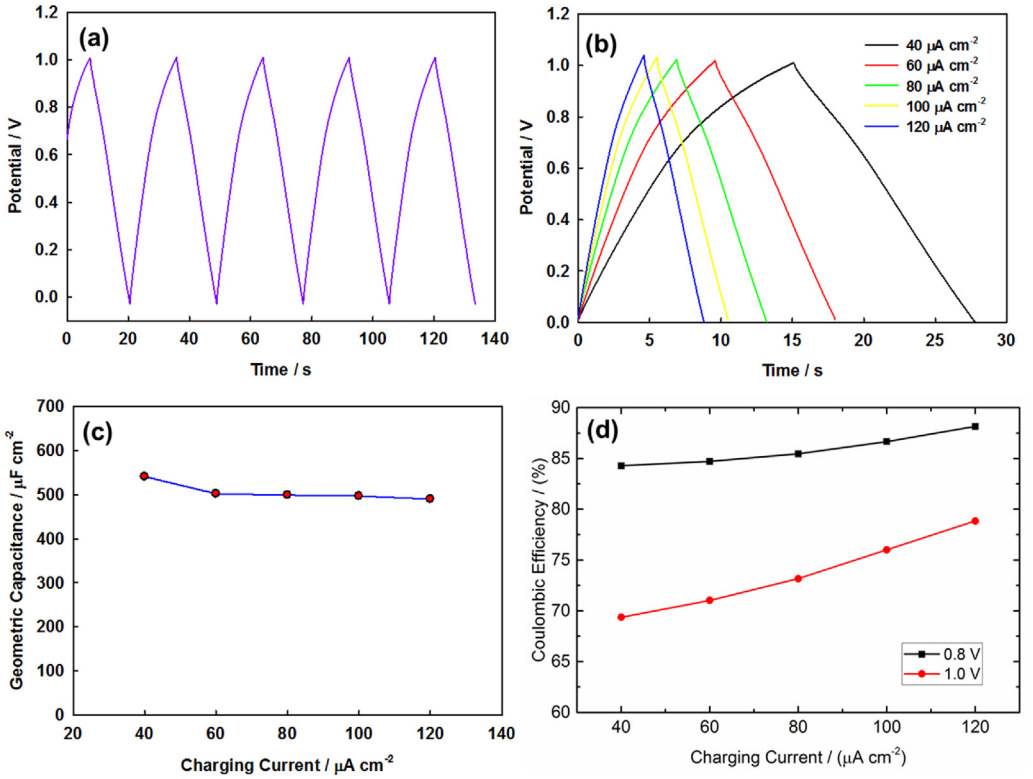

Fig. 6. (a) Galvanostatic charge-discharge curves for the $CoFe_2O_4$ symmetric supercapacitor device in 1 M NaOH aqueous electrolyte at a 40 μA charging current. (b) Galvanostatic charge-discharge curves at various charging currents. (c) plot of areal capacitance as a function of charging current. (d) Coulombic efficiency at various charging currents at maximum charging voltages of 0.8 V and 1.0 V.

for a bare FTO substrate and a $CoFe_2O_4$ film deposited at 500 °C on an identical FTO substrate (Fig. 4). The real axis intercept at high frequency is termed the solution resistance (resistance between the electrode-electrolyte interface), R_s. The value of R_s depends on the conductivity of the electrolyte as well as the electrode material. The R_s was estimated to be about 15.0 Ω for the $CoFe_2O_4$ film deposited on FTO substrate. Given that the estimated R_s of a bare FTO substrate was 11.8 Ω, the contribution of the $CoFe_2O_4$ film to the overall R_s was estimated to be about 3.2 Ω. The $CoFe_2O_4$ thin film exhibited Warburg behavior at high frequency, indicating diffusion resistance through the porous nanostructure within these timescales.

To assess the supercapacitor properties of the $CoFe_2O_4$ films, symmetrical cells with a two-electrode configuration were constructed as described in the experimental section to simulate supercapacitor device behaviour, using an aqueous 1 M NaOH electrolyte. The performance of the device was analysed by cyclic voltammetry up to a maximum voltage window of 1 V, between scan rates of 0.1 and 15 V/s; the CVs are shown in Fig. 5. The CVs showed quasi-rectangular behaviour up to 5 V/s, which demonstrated the high rate capability of the $CoFe_2O_4$ electrodes. At scan rates above the 5 V/s, the plot of discharge current density vs. scan rate starts to show deviation from linearity indicating inefficient charging of the electrodes beyond that scan rate. This is a direct consequence of the porous nature of the $CoFe_2O_4$ electrode. If the films were thicker and more porous, the deviation from linearity would occur at slower scan rates, indicating a slower rate capability. The CVs at faster scan rates of 5, 10 and 15 V/s can be seen in Fig. S5 in the supporting information.

As shown in Fig. 6a, the galvanostatic charge-discharge measurements show linear behavior up to a maximum voltage of 1 V, which demonstrates the characteristic behavior of an ideal capacitor. Galvanostatic charge-discharge measurements were also carried out at different charging currents ranging from 40–120 μA cm^{-2}, they are shown in Fig. 6b. The areal capacitance, determined from the slope of the discharge curve after the initial potential drop due to resistance, is shown in Fig. 6c for the same range of charging currents. An areal capacitance of 540 μF cm^{-2} is observed at a charging current of 40 μA cm^{-2}, but this slightly decreases to 500 μF cm^{-2} when 120 μA cm^{-2} is used. The fact that the capacitance drops only by 7.5% when the charging current density is increased from 40 to 120 μA cm^{-2} indicates that the supercapacitor has a good rate capability. The capacitance could not be expressed gravimetrically as the mass loading of the thin films could not be measured on a 4 decimal place balance. The coulombic efficiency (η) of the supercapacitor can be determined from the galvanostatic charge-discharge measurements using the

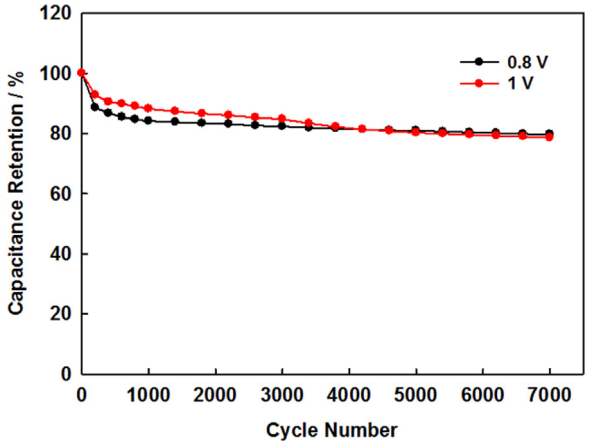

Fig. 7. Stability measurements of a symmetric $CoFe_2O_4$ supercapacitor measured with a charging current density of 120 μA cm^{-2}.

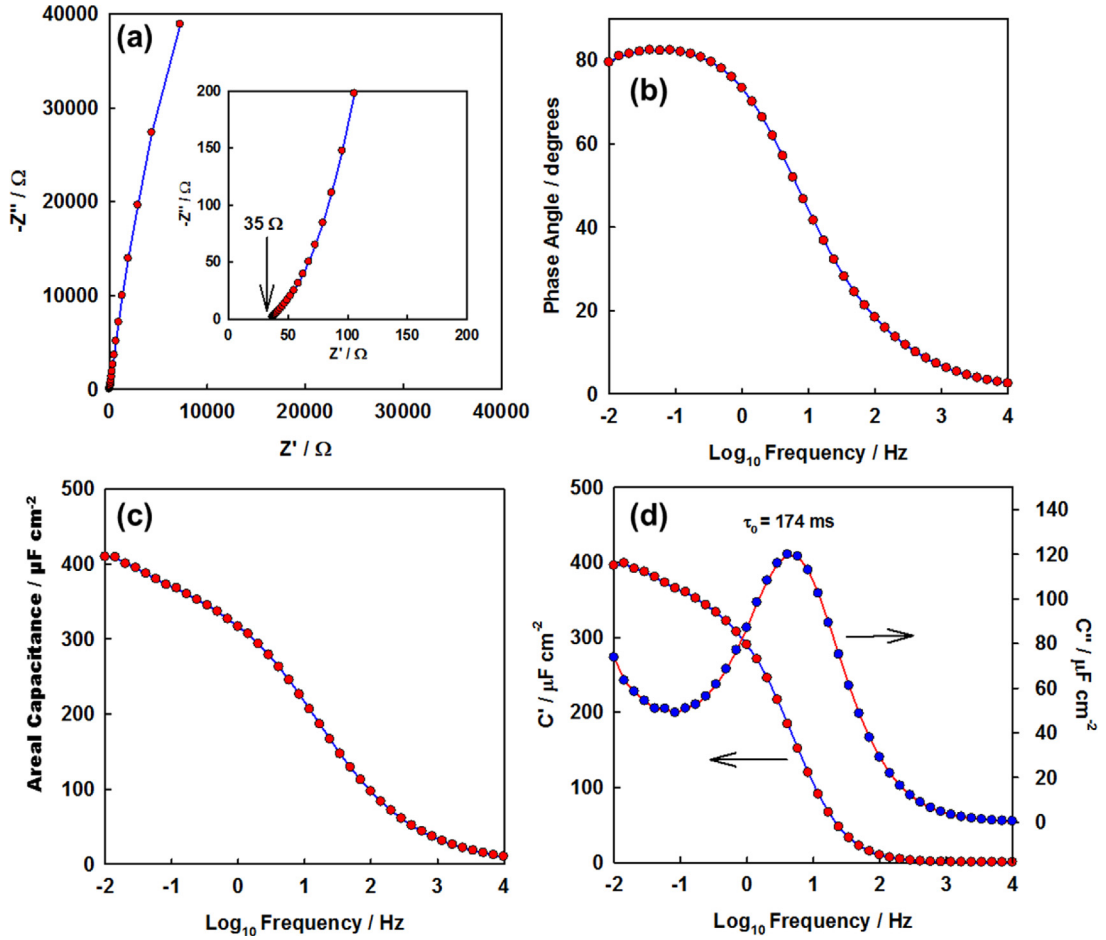

Fig. 8. (a) Nyquist plot for the $CoFe_2O_4$ symmetric supercapacitor; the inset shows an expanded region of the plot at high frequency. (b) phase angle as a function of frequency. (c) Areal capacitance as a function of frequency. (d) Imaginary and real areal capacitance as a function of frequency.

equation $\eta=\Delta t_d/\Delta t_c$ where t_d and t_c is the time taken to fully discharge and charge the capacitor, respectively. Fig. 6d shows the coulombic efficiency of the $CoFe_2O_4$ based supercapacitor at different charging currents. When the supercapacitor is charged to 1 V, the coulombic efficiency was 69% at a charging current of 40 $\mu A\,cm^{-2}$; however, the coulombic efficiency is increased to 79% as the charging current was increased to 120 $\mu A\,cm^{-2}$. $CoFe_2O_4$ is also an efficient OER catalyst [32], and the fairly low coulombic efficiency of $CoFe_2O_4$ stems from the fact that whilst it is working as a supercapacitor electrode, it also catalyzes the OER reaction in the 1 M NaOH electrolyte used in this work. Hence, a proportion of the charging current is going towards the OER reaction. The increase in the coulombic efficiency when the supercapacitor was charged at higher current densities could be due to the sluggish kinetics of OER [53]. Therefore, it is beneficial that the supercapacitor has a high rate capability as faster charging using higher current densities will reduce the OER side reaction. It was initially thought that the poor coulombic efficiencies of $CoFe_2O_4$ when charged to 1 V may limit its application in real devices, therefore charge-discharge measurements were also conducted at a lower voltage window of 0.8 V to see the difference in coulombic efficiency. When charged to 0.8 V, a higher coulombic efficiency of 83% was observed at a charging current of 40 $\mu A\,cm^{-2}$; this was further increased to 88% as the charging current was increased to 120 $\mu A\,cm^{-2}$.

The stability data of the 2-electrode cell at maximum charging voltages of 0.8 V and 1 V are shown in Fig. 7 at a charging current of 120 $\mu A\,cm^{-2}$. From this it can be seen that the capacitance drops by around 20% after 7000 cycles for both maximum charging potentials (0.8 V and 1 V). As this supercapacitor was completely sealed to prevent evaporation of the solvent, the decrease in capacitance is most likely to be due to the electrolyte decomposition by the OER. As the capacitance loss for the 0.8 V and 1 V supercapacitors was very similar (20% over 7000 cycles), this shows that a maximum charging voltage of 1 V is suitable for a symmetric $CoFe_2O_4$ supercapacitor. Also, the remarkable stability of $CoFe_2O_4$ over 7000 cycles demonstrates the good reversibility of the redox processes in $CoFe_2O_4$. This cycling stability is similar to other materials in the ferrite class of materials, for example $CuFe_2O_4$ and $ZnFe_2O_4$ [25,54].

The $CoFe_2O_4$ based supercapacitor was evaluated by EIS, and the Nyquist plot is shown in Fig. 8a. The Nyquist plot shows a near vertical linear line with a 45° line which intersects the real axis (Warburg element) which is typically observed for porous electrodes. The equivalent series resistance (ESR), determined from the high frequency real axis intercept, was 35 Ω. The ESR of 35 Ω agrees well with the three-electrode EIS measurements which showed that the R_s for a single $CoFe_2O_4$ electrode was 15.0 Ω. This indicates that approximately 30 Ω stems from the resistances of the two electrodes, and the remaining 5 Ω could stem from the separator. A plot of phase angle as a function of the frequency is shown in Fig. 8b. The closer the phase angle approaches to 90°, the more the device behaves like an ideal capacitor. In this case, a phase angle of 80° at 0.1 Hz was observed, which is very close to the ideal behaviour.

As the Nyquist plot showed vertical line capacitive behaviour, a series-RC circuit model was used to simulate the capacitive and resistive elements of the supercapacitor. In this model, the resistance is the real part of the impedance spectrum, and the capacitance is determined using the equation $C = -1/(2\pi f Z'')$, where f is the frequency in Hz and Z'' is the imaginary part of the impedance spectrum [55]. A plot of the areal capacitance as a function of the frequency is shown in Fig. 8c, in which the capacitance increases from 10 $\mu F\,cm^{-2}$ at 10 kHz to 415 $\mu F\,cm^{-2}$ at 0.01 Hz. The imaginary component of the capacitance was separated from the real component and both were plotted as a function of frequency, as shown in Fig. 8d. The maximum of the imaginary component of the capacitance can be used to determine the relaxation time constant, τ_0, which is the minimum time required to discharge all the energy from the device with an efficiency of greater than 50% of its maximum value: $\tau_0 = 1/f_{max}$. The τ_0 of the $CoFe_2O_4$ based supercapacitor was found to be 174 ms. This small τ_0 is another indication for the fast and efficient ion diffusion through the $CoFe_2O_4$ film. The areal energy and power densities of the $CoFe_2O_4$ supercapacitor were calculated to be $2.70 \times 10^{-4}\,J\,cm^{-2}$ and $7.14 \times 10^{-3}\,W\,cm^{-2}$, respectively.

4. Conclusions

High surface area nanostructured $CoFe_2O_4$ thin films were prepared by AACVD and were studied for application in supercapacitors. The $CoFe_2O_4$ was phase pure, and SEM analysis showed that the thin film morphology consisted of $CoFe_2O_4$ nanoparticles less than 100 nm in size that were sintered together to form larger dendrites ranging from 0.5–1 μm in diameter. Three-electrode electrochemical measurements revealed that $CoFe_2O_4$ is pseudocapacitive. $CoFe_2O_4$ electrodes were also tested in a two-electrode symmetric supercapacitor configuration and showed a capacitance of 540 $\mu F\,cm^{-2}$ and a time constant as small as 174 ms. The supercapacitor showed a capacitance retention of 80% after 7000 cycles indicating that the pseudocapacitive processes in $CoFe_2O_4$ are highly reversible and that it exhibits excellent electrochemical stability in 1 M NaOH alkaline electrolyte solution. We attribute the origin of pseudocapacitance to FeOOH and CoOOH surface groups. Our findings provide a much needed cheap alternative pseudocapacitive material to replace expensive materials such as IrO_2 and RuO_2.

Acknowledgements

All authors acknowledge the support given by the members of ERL to successfully conduct this research. JS and KGUW acknowledge the support from UK EPSRC (EP/L017709/1). AAT contributed to the initial work of this investigation in 2011 when he was a member of the ERL team and working under the project funded by EPSRC EP/F057342/1. The authors acknowledge use of facilities within the Loughborough Materials Characterisation Centre (LMCC). We would also like to thank Patricia Cropper for her assistance in obtaining XPS measurements.

Appendix A. Supplementary data

Supplementary data associated with this article can be found, in the online version, at **http://dx.doi.org/10.1016/j.electacta.2017.06.110**.

References

[1] B.E. Conway, Electrochemical Supercapacitors – Scientific Fundamentals and Technological Applications, Springer, 1999.
[2] S. Zhang, C. Peng, K.C. Ng, G.Z. Chen, Nanocomposites of manganese oxides and carbon nanotubes for aqueous supercapacitor stacks, Electrochim. Acta 55 (2010) 7447–7453, doi:http://dx.doi.org/10.1016/j.electacta.2010.01.078.
[3] Q. Qu, P. Zhang, B. Wang, Y. Chen, S. Tian, Y. Wu, R. Holze, Electrochemical Performance of MnO 2 Nanorods in Neutral Aqueous Electrolytes as a Cathode for Asymmetric Supercapacitors, J. Phys. Chem. C 113 (2009) 14020–14027, doi:http://dx.doi.org/10.1021/jp8113094.
[4] D.-Q. Liu, S.-H. Yu, S.-W. Son, S.-K. Joo, Electrochemical Performance of Iridium Oxide Thin Film for Supercapacitor Prepared by Radio Frequency Magnetron Sputtering Method, ECS Trans., ECS, 2008, pp. 103–109, doi:http://dx.doi.org/10.1149/1.2985632.
[5] G. Wee, H.Z. Soh, Y.L. Cheah, S.G. Mhaisalkar, M. Srinivasan, Synthesis and electrochemical properties of electrospun V2O5 nanofibers as supercapacitor electrodes, J. Mater. Chem. 20 (2010) 6720, doi:http://dx.doi.org/10.1039/c0jm00059k.
[6] C.-C. Hu, K.-H. Chang, M.-C. Lin, Y.-T. Wu, Design and tailoring of the nanotubular arrayed architecture of hydrous RuO2 for next generation supercapacitors, Nano Lett. 6 (2006) 2690–2695, doi:http://dx.doi.org/10.1021/nl061576a.
[7] S. Devaraj, N. Munichandraiah, High Capacitance of Electrodeposited MnO[sub 2] by the Effect of a Surface-Active Agent, Electrochem. Solid-State Lett. 8 (2005) A373, doi:http://dx.doi.org/10.1149/1.1922869.
[8] S.-C. Pang, M.A. Anderson, T.W. Chapman, Novel Electrode Materials for Thin-Film Ultracapacitors: Comparison of Electrochemical Properties of Sol-Gel-Derived and Electrodeposited Manganese Dioxide, J. Electrochem. Soc. 147 (2000) 444, doi:http://dx.doi.org/10.1149/1.1393216.
[9] M. Toupin, T. Brousse, D. Bélanger, Charge Storage Mechanism of MnO 2 Electrode Used in Aqueous Electrochemical Capacitor, Chem. Mater. 16 (2004) 3184–3190, doi:http://dx.doi.org/10.1021/cm049649j.
[10] J.-K. Chang, M.-T. Lee, W.-T. Tsai, In situ Mn K-edge X-ray absorption spectroscopic studies of anodically deposited manganese oxide with relevance to supercapacitor applications, J. Power Sources. 166 (2007) 590–594, doi:http://dx.doi.org/10.1016/j.jpowsour.2007.01.036.
[11] M. Toupin, T. Brousse, D. Bélanger, Influence of Microstucture on the Charge Storage Properties of Chemically Synthesized Manganese Dioxide, Chem. Mater. 14 (2002) 3946–3952, doi:http://dx.doi.org/10.1021/cm020408q.
[12] C. Gopal Reddy, Semiconducting gas sensor for chlorine based on inverse spinel nickel ferrite, Sensors Actuators B Chem. 55 (1999) 90–95, doi:http://dx.doi.org/10.1016/S0925-4005(99)00112-4.
[13] M.G. Chapline, S.X. Wang, Room-temperature spin filtering in a CoFe2O4/MgAl2O4/Fe3O4 magnetic tunnel barrier, Phys. Rev. B 74 (2006) 14418, doi:http://dx.doi.org/10.1103/PhysRevB.74.014418.
[14] S. Lee, A. Fursina, J.T. Mayo, C.T. Yavuz, V.L. Colvin, R.G.S. Sofin, I.V. Shvets, D. Natelson, Electrically driven phase transition in magnetite nanostructures, Nat. Mater. 7 (2008) 130–133, doi:http://dx.doi.org/10.1038/nmat2084.
[15] M.J. Carey, S. Maat, P. Rice, R.F.C. Farrow, R.F. Marks, A. Kellock, P. Nguyen, B.A. Gurney, Spin valves using insulating cobalt ferrite exchange-spring pinning layers, Appl. Phys. Lett. 81 (2002) 1044–1046.
[16] G.A. Prinz, Magnetoelectronics, Science (80-.) 282 (1998) 1660–1663, doi:http://dx.doi.org/10.1126/science.282.5394.1660.
[17] S.A. Wolf, D.D. Awschalom, R.A. Buhrman, J.M. Daughton, S. von Molnár, M.L. Roukes, A.Y. Chtchelkanova, D.M. Treger, Spintronics: a spin-based electronics vision for the future, Science 294 (2001) 1488–1495, doi:http://dx.doi.org/10.1126/science.1065389.
[18] Z. He, J.A. Koza, G. Mu, A.S. Miller, E.W. Bohannan, J.A. Switzer, Electrodeposition of Co x Fe 3-x O 4 Epitaxial Films and Superlattices, Chem. Mater 25 (2013) 223–232, doi:http://dx.doi.org/10.1021/cm303289t.
[19] R. Rennard, Oxidative dehydrogenation of butenes over ferrite catalysts, J. Catal. 21 (1971) 282–293, doi:http://dx.doi.org/10.1016/0021-9517(71)90147-3.
[20] V.S. Kumbhar, A.D. Jagadale, N.M. Shinde, C.D. Lokhande, Chemical synthesis of spinel cobalt ferrite (CoFe2O4) nano-flakes for supercapacitor application, Appl. Surf. Sci. 259 (2012) 39–43, doi:http://dx.doi.org/10.1016/j.apsusc.2012.06.034.
[21] D. Zha, P. Xiong, X. Wang, Strongly coupled manganese ferrite/carbon black/polyaniline hybrid for low-cost supercapacitors with high rate capability, Electrochim. Acta 185 (2015) 218–228, doi:http://dx.doi.org/10.1016/j.electacta.2015.10.139.
[22] P. Xiong, C. Hu, Y. Fan, W. Zhang, J. Zhu, X. Wang, Ternary manganese ferrite/graphene/polyaniline nanostructure with enhanced electrochemical capacitance performance, J. Power Sources 266 (2014) 384–392, doi:http://dx.doi.org/10.1016/j.jpowsour.2014.05.048.
[23] K.V. Sankar, R.K. Selvan, The ternary MnFe2O4/graphene/polyaniline hybrid composite as negative electrode for supercapacitors, J. Power Sources 275 (2015) 399–407, doi:http://dx.doi.org/10.1016/j.jpowsour.2014.10.183.
[24] Z.-Y. Yu, L.-F. Chen, S.-H. Yu, Growth of NiFe2O4 nanoparticles on carbon cloth for high performance flexible supercapacitors, J. Mater. Chem. A 2 (2014) 10889, doi:http://dx.doi.org/10.1039/c4ta00492b.
[25] M.M. Vadiyar, S.C. Bhise, S.S. Kolekar, J.-Y. Chang, K.S. Ghule, A.V. Ghule, Low cost flexible 3-D aligned and cross-linked efficient ZnFe2O4 nano-flakes electrode on stainless steel mesh for asymmetric supercapacitors, J. Mater. Chem. A 4 (2016) 3504–3512, doi:http://dx.doi.org/10.1039/C5TA09022A.
[26] L. Li, H. Bi, S. Gai, F. He, P. Gao, Y. Dai, X. Zhang, D. Yang, M. Zhang, P. Yang, Uniformly Dispersed ZnFe2O4 Nanoparticles on Nitrogen-Modified Graphene for High-Performance Supercapacitor as Electrode, Sci. Rep. 7 (2017) 43116, doi:http://dx.doi.org/10.1038/srep43116.

[27] W. Zhang, B. Quan, C. Lee, S.-K. Park, X. Li, E. Choi, G. Diao, Y. Piao, One-Step Facile Solvothermal Synthesis of Copper Ferrite–Graphene Composite as a High-Performance Supercapacitor Material, ACS Appl. Mater. Interfaces 7 (2015) 2404–2414, doi:http://dx.doi.org/10.1021/am507014w.
[28] V.S. Kumbhar, A.D. Jagadale, N.M. Shinde, C.D. Lokhande, Chemical synthesis of spinel cobalt ferrite (CoFe2O4) nano-flakes for supercapacitor application, Appl. Surf. Sci. 259 (2012) 39–43, doi:http://dx.doi.org/10.1016/j.apsusc.2012.06.034.
[29] L. Lv, Q. Xu, R. Ding, L. Qi, H. Wang, Chemical synthesis of mesoporous CoFe2O4 nanoparticles as promising bifunctional electrode materials for supercapacitors, Materials Letters 111 (15) (2013) 35–38, doi:http://dx.doi.org/10.1016/j.matlet.2013.08.055.
[30] P. Xiong, H. Huang, X. Wang, Design and synthesis of ternary cobalt ferrite/graphene/polyaniline hierarchical nanocomposites for high-performance supercapacitors, J. Power Sources 245 (2014) 937–946, doi:http://dx.doi.org/10.1016/j.jpowsour.2013.07.064.
[31] J. Hao, W. Yang, Z. Zhang, B. Lu, B. Zhang, J. Tang, Facile Synthesis of 3D Hierarchical Flower-like Co3-xFexO4 ferrite on Nickel Foam as High-Performance Electrodes for Supercapacitors, Electrochim. Acta 152 (2015) 13–18, doi:http://dx.doi.org/10.1016/j.electacta.2014.11.104.
[32] A. Kargar, S. Yavuz, T.K. Kim, C.-H. Liu, C. Kuru, C.S. Rustomji, S. Jin, P.R. Bandaru, Solution-Processed CoFe2O4 Nanoparticles on 3D Carbon Fiber Papers for Durable Oxygen Evolution Reaction, ACS Appl. Mater. Interfaces 7 (2015) 17851–17856, doi:http://dx.doi.org/10.1021/acsami.5b04270.
[33] L. Guan, L. Yu, G.Z. Chen, Capacitive and non-capacitive faradaic charge storage, Electrochim. Acta. 206 (2016) 464–478, doi:http://dx.doi.org/10.1016/j.electacta.2016.01.213.
[34] A.A. Tahir, M.A. Ehsan, M. Mazhar, K.G.U. Wijayantha, M. Zeller, A.D. Hunter, Photoelectrochemical and Photoresponsive Properties of Bi 2S 3 Nanotube and Nanoparticle Thin Films, Chem. Mater. 22 (2010) 5084–5092, doi:http://dx.doi.org/10.1021/cm101642b.
[35] R. Dharmadasa, A.A. Tahir, K.G.U. Wijayantha, Single Step Growth and Characterization of Zinc Oxide, Tin Oxide, and Composite (Zn x Sn 1-x O y) Nanoplate and Nanocolumn Electrodes, J. Am. Ceram. Soc. 94 (2011) 3540–3546, doi:http://dx.doi.org/10.1111/j.1551-2916.2011.04525.x.
[36] M.D. Stoller, R.S. Ruoff, Best practice methods for determining an electrode material's performance for ultracapacitors, Energy Environ. Sci. 3 (2010) 1294, doi:http://dx.doi.org/10.1039/c0ee00074d.
[37] M. George, S.S. Nair, K.A. Malini, P.A. Joy, M.R. Anantharaman, Finite size effects on the electrical properties of sol-gel synthesized CoFe2O4 powders: deviation from Maxwell–Wagner theory and evidence of surface polarization effects, J. Phys. D. Appl. Phys. 40 (2007) 1593–1602, doi:http://dx.doi.org/10.1088/0022-3727/40/6/001.
[38] M. Sangmanee, S. Maensiri, Nanostructures and magnetic properties of cobalt ferrite (CoFe2O4) fabricated by electrospinning, Appl. Phys. A 97 (2009) 167–177, doi:http://dx.doi.org/10.1007/s00339-009-5256-5.
[39] C. Cannas, A. Falqui, A. Musinu, D. Peddis, G. Piccaluga, CoFe2O4 nanocrystalline powders prepared by citrate-gel methods: Synthesis, structure and magnetic properties, J. Nanoparticle Res. 8 (2006) 255–267, doi:http://dx.doi.org/10.1007/s11051-005-9028-7.
[40] K. Maaz, A. Mumtaz, S.K. Hasanain, A. Ceylan, Synthesis and magnetic properties of cobalt ferrite (CoFe2O4) nanoparticles prepared by wet chemical route, J. Magn. Magn. Mater. 308 (2007) 289–295, doi:http://dx.doi.org/10.1016/j.jmmm.2006.06.003.
[41] I.H. Gul, A. Maqsood, Structural, magnetic and electrical properties of cobalt ferrites prepared by the sol–gel route, J. Alloys Compd. 465 (2008) 227–231, doi:http://dx.doi.org/10.1016/j.jallcom.2007.11.006.
[42] P. Chandramohan, M.P. Srinivasan, S. Velmurugan, S.V. Narasimhan, Cation distribution and particle size effect on Raman spectrum of CoFe2O4, J. Solid State Chem. 184 (2011) 89–96, doi:http://dx.doi.org/10.1016/j.jssc.2010.10.019.
[43] D. Gu, C.-J. Jia, C. Weidenthaler, H.-J. Bongard, B. Spliethoff, W. Schmidt, F. Schüth, Highly Ordered Mesoporous Cobalt-Containing Oxides: Structure, Catalytic Properties, and Active Sites in Oxidation of Carbon Monoxide, J. Am. Chem. Soc. 137 (2015) 11407–11418, doi:http://dx.doi.org/10.1021/jacs.5b06336.
[44] N.V. Long, Y. Yang, T. Teranishi, C.M. Thi, Y. Cao, M. Nogami, Related magnetic properties of CoFe2O4 cobalt ferrite particles synthesised by the polyol method with NaBH4 and heat treatment: new micro and nanoscale structures, RSC Adv. 5 (2015) 56560–56569, doi:http://dx.doi.org/10.1039/C5RA10015A.
[45] S. Saremi-Yarahmadi, K.G.U. Wijayantha, A.A. Tahir, B. Vaidhyanathan, Nanostructured α-Fe2O3 Electrodes for Solar Driven Water Splitting: Effect of Doping Agents on Preparation and Performance, J. Phys. Chem. C 113 (2009) 4768–4778, doi:http://dx.doi.org/10.1021/jp808453z.
[46] A.A. Tahir, K.G.U. Wijayantha, Photoelectrochemical water splitting at nanostructured ZnFe2O4 electrodes, J. Photochem. Photobiol. A Chem. 216 (2010) 119–125, doi:http://dx.doi.org/10.1016/j.jphotochem.2010.07.032.
[47] A.A. Tahir, H.A. Burch, K.G.U. Wijayantha, B.G. Pollet, A new route to control texture of materials: Nanostructured ZnFe2O4 photoelectrodes, Int. J. Hydrogen Energy 38 (2013) 4315–4323, doi:http://dx.doi.org/10.1016/j.ijhydene.2013.01.130.
[48] A.A. Tahir, M.A. Ehsan, M. Mazhar, K.G.U. Wijayantha, M. Zeller, A.D. Hunter, Photoelectrochemical and photoresponsive properties of Bi2S 3 nanotube and nanoparticle thin films, Chem. Mater. 22 (2010), doi:http://dx.doi.org/10.1021/cm101642b.
[49] G. Huo, X. Lu, Y. Huang, W. Li, G. Liang, Electrochemical Performance of −Fe2O3 Particles as Anode Material for Aqueous Rechargeable Batteries, J. Electrochem. Soc. 161 (2014) A1144–A1148, doi:http://dx.doi.org/10.1149/2.077406jes.
[50] J.S. Sagu, K.G.U. Wijayantha, M. Bohm, S. Bohm, T. Kumar Rout, Anodized Steel Electrodes for Supercapacitors, ACS Appl. Mater. Interfaces 8 (2016) 6277–6285, doi:http://dx.doi.org/10.1021/acsami.5b12107.
[51] L. Ma, H. Zhou, X. Shen, Q. Chen, G. Zhu, Z. Ji, Facile synthesis of Co3O4 porous nanosheets/reduced graphene oxide composites and their excellent supercapacitor performance, RSC Adv. 4 (2014) 53180–53187, doi:http://dx.doi.org/10.1039/C4RA07136K.
[52] M.S. Burke, M.G. Kast, L. Trotochaud, A.M. Smith, S.W. Boettcher, Cobalt-iron (oxy)hydroxide oxygen evolution electrocatalysts: the role of structure and composition on activity, stability, and mechanism, J. Am. Chem. Soc. 137 (2015) 3638–3648, doi:http://dx.doi.org/10.1021/jacs.5b00281.
[53] L.M. Peter, K.G. Upul Wijayantha, Photoelectrochemical Water Splitting at Semiconductor Electrodes: Fundamental Problems and New Perspectives, ChemPhysChem 15 (2014) 1983–1995, doi:http://dx.doi.org/10.1002/cphc.201402024.
[54] W. Zhang, B. Quan, C. Lee, S.-K. Park, X. Li, E. Choi, G. Diao, Y. Piao, One-Step Facile Solvothermal Synthesis of Copper Ferrite–Graphene Composite as a High-Performance Supercapacitor Material, ACS Appl. Mater. Interfaces 7 (2015) 2404–2414, doi:http://dx.doi.org/10.1021/am507014w.
[55] P.L. Taberna, P. Simon, J.F. Fauvarque, Electrochemical Characteristics and Impedance Spectroscopy Studies of Carbon-Carbon Supercapacitors, J. Electrochem. Soc. 150 (2003) A292, doi:http://dx.doi.org/10.1149/1.1543948.